PNNL-SA-124478

Pacific Northwest
NATIONAL LABORATORY

Flux-assisted CdTe and CdSe growth using an in situ dynamic-flux-removal process

November 2018

BJ Riley
CH Henager, Jr.
DW Matson
NR Overman
DA Pierce

U.S. DEPARTMENT OF ENERGY

Prepared for the U.S. Department of Energy
under Contract DE-AC05-76RL01830

DISCLAIMER

PACIFIC NORTHWEST NATIONAL LABORATORY
operated by
BATTELLE
for the
UNITED STATES DEPARTMENT OF ENERGY
under Contract DE-AC05-76RL01830

Printed in the United States of America

Available to DOE and DOE contractors from the
Office of Scientific and Technical Information,
P.O. Box 62, Oak Ridge, TN 37831-0062;
ph: (865) 576-8401
fax: (865) 576-5728
email: reports@adonis.osti.gov

Available to the public from the National Technical Information Service
5301 Shawnee Rd., Alexandria, VA 22312
ph: (800) 553-NTIS (6847)
email: orders@ntis.gov <http://www.ntis.gov/about/form.aspx>
Online ordering: http://www.ntis.gov

PNNL-SA-124478

Flux-assisted CdTe and CdSe growth using an in situ dynamic-flux-removal process

Subtitle

November 2018

BJ Riley
CH Henager, Jr.
DW Matson
NR Overman
DA Pierce

Prepared for
the U.S. Department of Energy
under Contract DE-AC05-76RL01830

Pacific Northwest National Laboratory
Richland, Washington 99352

Abstract

A flux-assisted in situ dynamic-flux-removal process for growing CdTe and CdSe using a getter metal is discussed. A metal getter (e.g., stainless steel, Pt, Cu, Ni, and Ag) was placed in the annulus outside of a glassy carbon crucible containing the CdTe+Te or CdSe+Se and this was sealed within an evacuated fused quartz ampoule. The excess Te and Se were added as fluxes. After melting, the flux and some Cd(Te,Se) was removed from the crucible through volatility and reacted with the metal getter forming metal tellurides. This process was conducted at temperatures below the melting temperatures of CdTe (T_m ~1041 °C) and CdSe (T_m ~1268 °C) and once the flux was removed, the CdTe or CdSe solidified into a solid polycrystalline ingot with several large grains. Following a 24-hr soak, different cooling rates were used including 0.1 °C min^{-1}, 1 °C min^{-1}, as well as furnace, air, and water quenching. The slowest quench rate (0.1 °C min^{-1}) yielded the largest-grained crystals for the CdTe experiments. This process was then demonstrated in a gradient furnace using Cu and Ni getters to grow CdTe samples of ~100 g. The experiments conducted for CdSe were not as successful as for CdTe, yielding products of smaller grain sizes than were achieved with CdTe.

Acknowledgments

The Pacific Northwest National Laboratory is operated for the U.S. Department of Energy by Battelle Memorial Institute under contract DE-AC06-76RLO 1830. This work was funded by the Office of Defense Nuclear Nonproliferation, Office of Nonproliferation Research and Development (NA-22), under contract DE-AC05-00OR-22725 with UT-Battelle, LLC. Authors thank Ryan Brown from Keyence for help collecting some of the images. Authors thank Clyde Chamberlin and Anthony Guzman for preparing samples for analysis. Authors also thank Brad Johnson for helpful support.

Acronyms and Abbreviations

AQ	air quench
CdSe	cadmium selenide
CdTe	cadmium telluride
EBSD	electron backscatter diffraction
EDS	energy dispersive spectroscopy
FC	furnace cool
IPF	inverse pole figure
ITF	isothermal temperature furnace
Max	maximum
Min	minimum
P-XRD	powder X-ray diffraction
SEM	scanning electron microscopy
SS	stainless steel
St. Dev.	standard deviation
T_m	melting temperature
T_s	soak temperature
VGF	vertical gradient furnace
WQ	water quench

Contents

Abstract iii
Acknowledgments v
Acronyms and Abbreviations vii
1.0 Introduction 1.1
2.0 Experimental Methods 2.1
2.1 CdTe experiments 2.1
2.2 CdSe experiments 2.1
2.3 Isothermal furnace (ITF) experiments 2.1
2.4 Vertical gradient furnace (VGF) experiments 2.2
2.5 Post heat-treatment sample preparations 2.2
2.6 Powder X-ray diffraction 2.2
2.7 Optical microscopy 2.2
2.8 Electron backscatter diffraction 2.3
3.0 Results and Discussion 3.1
3.1 CdTe experiments 3.1
3.1.1 ITF experiments 3.1
3.1.2 VGF experiments 3.5
3.2 CdSe experiments 3.6
4.0 Conclusions 4.1
5.0 References 5.1
Appendix A – EDS Analysis of Getter Concentrations in CdTe Crystals A.1

Figures

Figure 1-1. Location of $Cd_{30}Te_{70}$ on the CdTe binary phase diagram after Greenberg (Greenberg, 2003) where the region near the 50%/50% composition is enlarged in the dotted box. The pink dotted line at $Cd_{30}Te_{70}$ denotes where the experiments from the current work were performed. 1.2

Figure 1-2. Schematic showing the flux-assisted in situ dynamic flux removal process. 1.2

Figure 3-2. Pictures of ITF-1000C-FC-Pt-1 (ITF-1) both (a) before and (b,c) after the heat treatment. 3.1

Figure 3-3. Thermal profile for the different cooling rates used during the ITF experiments. 3.1

Figure 3-4. Optical collage of select samples. For scale, all samples are shown at ~10-mm diameter. 3.2

Figure 3-5. Annulus material phase distribution comparisons for (a) all getters run with 1 °C min^{-1} cooling rate and (b) for all Pt samples run at different cooling rates. For both plots, an overlay is provided for the amount of charge that was removed from the crucible into the annulus during the experiment. 3.4

Figure 3-6. (a) Optical micrograph of ITF-1000C-0.1C-Pt (RF-7). (b-e) EBSD collage collected over the region highlighted in (a) including (b) pattern quality map, (c) IPF-X map, (d) IPF-Y map, and (e) IPF-Z map (IPF = inverse pole figure). 3.5

Figure 3-7. Optical micrographs of (a) VGF-8x-1C-Cu (VGF-1) and (b) VGF-8x-1C-Ni (VGF-2). 3.5

Figure 3-8. Pictures of (a) CdSe-1 and (b) CdSe-2 and (c) an EBSD map (IPF-Z) collage across the CdSe crystal grains of one of the sections cut from CdSe-2. ..... 3.6

Figure A-1. EDS spectra from ITF-10 (Ni getter; EDS region 2). Locations of the primary Te and Ni peaks illustrate that summation of 2× the energy from a Te Lα peak very nearly overlaps the Ni Kα peak. A.7

Tables

Table 2-1. Summary of samples for ITF and VGF experiments. All samples were heated at a heating rate of 1 °C min^{-1}and 24-hr soak time at the specified soak temperature (T_s). ITF = isothermal temperature furnace, VGF = vertical gradient furnace, FC = furnace cool, WQ = water quench, AQ = air quench...... 2.1

Table 3-2. Summary of phases (Anderko and Schubert, 1954; Bradley, 1924; Davey, 1925; Dobrovol'skii et al., 1972; Forman and Peacock, 1949; Furberg, 1953; Hamasaki et al., 1975; Imanov and Pinsker, 1966; Peacock and Thompson, 1946; Pertlik, 1986; Thomassen, 1929; Woolley and Williams, 1966) present in material found outside the crucible in the annulus with P-XRD analysis where "SS" denotes stainless steel. For the VGF entries in the table, the top row designates the material found on top of the crucible lid and the bottom is what was found at the bottom tip of the annulus with masses for each shown in brackets "[ ]" under the 'Other' column...... 3.3

Table A-1. EDS Results for ITF-1000C-1C-Pt ($Cd_{70}Te_{30}$, ITF-5 with Pt-wire). A.3

Table A-2. EDS Results for ITF-1000C-1C-Cu ($Cd_{70}Te_{30}$, ITF-9 with Cu-wire). A.4

Table A-3. EDS Results for ITF-1000C-1C-Ni ($Cd_{70}Te_{30}$, ITF-10 with Ni-Wire).** A.5

Table A-4. EDS Results for ITF-1000C-1C-Ag ($Cd_{70}Te_{30}$, ITF-11 with Ag-Wire). A.6

Table A-5. Forced Ni background measured from ITF-5, ITF-9, and ITF-11. ..... A.8

Table A-6. ITF-10 (Ni getter) background subtraction (Ni correction). A.9

Table A-7. Summary of getter concentrations measured by EDS. A.10

1.0 Introduction

Cadmium telluride (CdTe) is a semiconductor with a 1.52 eV band gap (300 K) (Knoll, 2000) with a wide range of applications including photovoltaics (Gessert and Bonnet, 2015), radiation detection (Becker et al., 2011; Burger et al., 2003), mid-infrared-transparency (Wald, 1977), electro-optical modulation (Johnson, 1968; Johnson et al., 1969), optical mixing (McArthur and McFarlane, 1970), continuous second harmonic generation (Stafsudd and Alexander, 1971), piezoelectrics (Berlincourt et al., 1963), and electroluminescent diodes (Mandel and Morehead, 1964). Some of these applications utilize dopants such as Zn, As, Hg, and In (Carmody and Gilmore, 2011; Henager et al., 2015; Schaake et al., 1985). Many CdTe applications require large single crystals that are grown using techniques such as Czochralski pulling (Triboulet and Siffert, 2010), vertical or horizontal Bridgman (Henager et al., 2015; Triboulet and Siffert, 2010), the traveling heater method (Shiraki et al., 2007; Triboulet and Siffert, 2010), and zone refining (Triboulet and Siffert, 2010; Woodbury and Lewandowski, 1971) while others utilize polycrystalline forms (Gessert and Bonnet, 2015), thin films, or even quantum dots (Wuister et al., 2003). Different techniques have been used to make CdTe-based products including chemical spraying, electrodeposition, vacuum sublimation, non-vacuum sublimation, non-vacuum printing, screen printing, sputtering, and hydrothermal approaches (Chu and Chu, 1993; Gessert and Bonnet, 2015; Triboulet and Siffert, 2010).

In some cases, CdTe crystals have also been grown using fluxes such as Bi, Sn, Cd, and Te (Rubenstein, 1966, 1968; Triboulet and Siffert, 2010). With the addition of a flux, processing temperatures below the melting temperature of the target crystals can be used for growth, which minimizes decomposition and volatility during processing, and can help if the system undergoes a phase transition at temperatures below the melting temperature (Koohpayeh, 2016). A drawback to flux-assisted growth is that crystals grow at slower rates (by ~100×) (Koohpayeh, 2016) due to the reduced temperature, but this can also lead to a reduced strain in the final product. An additional drawback is that the flux can be found at the grain boundaries of crystals (Henager et al., 2015). However, with flux-assisted growth being possible at lower temperatures, less sophisticated and costly equipment can be used to grow materials that typically require high temperatures.

In the work presented here, a flux-assisted growth process was used to grow CdTe crystals from a Te-rich solution of $Cd_{30}Te_{70}$ with a melting temperature of ~900 °C [see Figure 1-2 (Greenberg, 2003)]. While the flux-assisted crystal growth process is not unique, what is unique about the approach taken here is that high purity stainless steel, Pt, Cu, Ni, or Ag wires were added to the annular region between the crucible and the ampoule to act as getters for the excess Te, which was preferentially removed from the crucible during the experiment. A schematic of this process is shown in Figure 1-2. The authors believe that the process by which the flux is dynamically removed from the ampoule using a getter is a unique approach for growing single crystals of CdTe. While these crystals are not exceptionally large, the work presented here demonstrates the utility of such a process that could be extrapolated to other crystal systems.

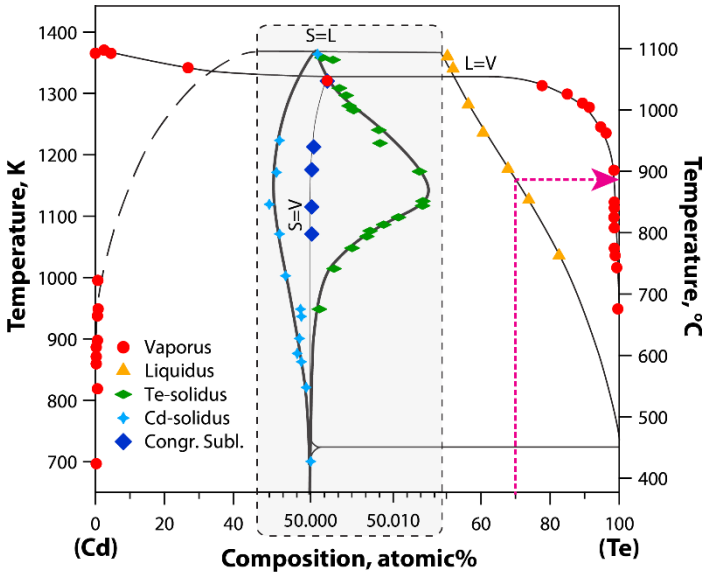

Figure 1-1. Location of $Cd_{30}Te_{70}$ on the CdTe binary phase diagram after Greenberg (2003) where the region near the 50%/50% composition is enlarged in the dotted box. The pink dotted line at $Cd_{30}Te_{70}$ denotes where the experiments from the current work were performed.

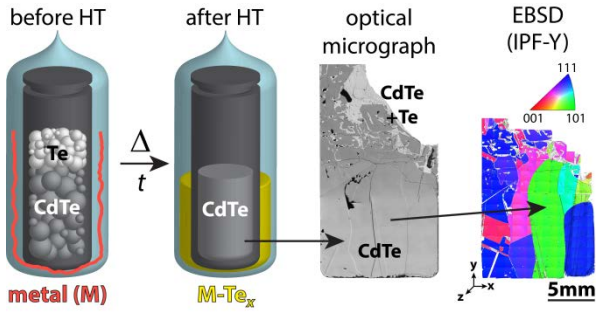

Figure 1-2. Schematic showing the flux-assisted in situ dynamic flux removal process.

Proof-of-concept experiments were also conducted for CdSe using a similar approach taken to grow the CdTe samples. While CdSe is often synthesized as quantum dots (Dabbousi et al., 1997) and various other nanocrystalline shapes including rods, arrows, teardrops, and tetrapods (Manna et al., 2000), Bridgman growth has been documented (Mongy, 2004). The beneficial applications of CdSe include room temperature radiation detection (Burger et al., 1983), non-linear optical properties (Park et al., 1993), and photoluminescence (Qu and Peng, 2002). Since CdSe melts at 1239-1258 °C (Cook, 1968; Sosovska, 2007), a notably higher temperature than CdTe (1092 °C) (Avetissov et al., 2011), this higher melting temperature poses restrictions on the type of growth process that can be conducted based on furnace limitations, temperature limitations of fused quartz vessels, component volatilities, and other safety hazards. Thus, an approach utilizing flux-assisted growth for making CdSe is attractive.

2.0 Experimental Methods

2.1 CdTe experiments

All CdTe samples were batched with an analytical balance (±0.1 mg) to an initial target composition of $Cd_{30}Te_{70}$ inside of a nitrogen glovebox (M-Braun, Waltham, CN) using 99.9999% CdTe and Te (5N Plus, Canada) with a target composition of $Cd_{30}Te_{70}$. The amounts of Pt, Cu, Ni, and Ag getters added based on the amount of Te reacted during the first experiment, ITF-1000C-FC-Pt-1 (ITF-1) and on the expected getter-telluride product compounds [$PtTe_2$ (T_m = 1147 °C) (Mangin and Veber, 2008), CuTe (T_m ~407 °C) (Okamoto and Massalski, 1994), $NiTe_2$ (T_m = 900.5 °C) (Lee and Nash, 1991), and Ag_2Te (T_m = 960 °C) (Karakaya and Thompson, 1991), respectively]. The details of sample masses, type and mass of getter used, soak temperature (T_s), and cooling method for each experiment are presented in Table 2-1.

Table 2-1. Summary of samples for ITF and VGF experiments. All samples were heated at a heating rate of 1 °C min^{-1}and 24-hr soak time at the specified soak temperature (T_s). ITF = isothermal temperature furnace, VGF = vertical gradient furnace, FC = furnace cool, WQ = water quench, AQ = air quench.

Sample ID	Alt. ID	Sample mass (g)				Metal getter	Getter mass (g)	T_s, (°C)	Cooling method
		CdTe	Te	CdSe	Se				
ITF-1000C-FC-Pt-1	ITF-1	7.60	5.39	-	-	Pt	2.43	1000	FC
ITF-1025C-FC-SS	ITF-2	7.59	5.38	-	-	SS	0.20	1025	FC
ITF-1000C-FC-SS	ITF-3	7.59	5.38	-	-	SS	0.20	1000	FC
ITF-1000C-FC-Pt-2	ITF-4	7.59	5.38	-	-	Pt	2.50	1000	FC
ITF-1000C-1C-Pt	ITF-5	7.60	5.38	-	-	Pt	2.48	1000	1 °C min^{-1}
ITF-1000C-WQ-Pt	ITF-6	7.60	5.39	-	-	Pt	2.70	1000	WQ
ITF-1000C-0.1C-Pt	ITF-7	7.60	5.39	-	-	Pt	2.70	1000	0.1 °C min^{-1}
ITF-1000C-AQ-Pt	ITF-8	7.59	5.38	-	-	Pt	2.70	1000	AQ
ITF-1000C-1C-Cu	ITF-9	7.59	5.39	-	-	Cu	1.76	1000	1 °C min^{-1}
ITF-1000C-1C-Ni	ITF-10	7.60	5.38	-	-	Ni	1.22	1000	1 °C min^{-1}
ITF-1000C-1C-Ag	ITF-11	7.60	5.38	-	-	Ag	5.96	1000	1 °C min^{-1}
VGF-8x-1C-Cu	VGF-1	122.40	86.77	-	-	Cu	28.32	1000-1050	1 °C min^{-1}
VGF-8x-1C-Ni	VGF-1	122.53	86.86	-	-	Ni	19.74	1000-1050	1 °C min^{-1}
ITF-CdSe-1.5x-10C-Pt	CdSe-1	-	-	7.20	3.96	Pt	3.20	1100	10°C min-1
ITF-CdSe-6x-0.003C	CdSe-2	-	-	30.00	4.37	-	-	1100	0.2°C hr-1

2.2 CdSe experiments

The CdSe experiments were prepared in the same fashion as the CdTe experiments but with an initial target composition of $Cd_{30}Se_{70}$ for CdSe-1 and $Cd_{42.5}Se_{57.5}$ for CdSe-2 using 99.999% CdSe (American Elements, Los Angeles, CA) and 99.999% Se (Alfa Aesar) for the chemicals (see Table 2-1). For CdSe-1, a Pt getter was used. For CdSe-2, the experiment was performed without a crucible at a lower Se flux loading to help reduce the likelihood of an ampoule overpressurization.

2.3 Isothermal furnace (ITF) experiments

For the isothermal furnace (ITF) experiments shown in Table 2-1, the raw materials were placed into a conical glassy carbon crucible (GAZ-06, HTW Hochtemperatur-Werkstoffe GmbH, Germany), a glassy carbon lid was added to the crucible, and then the crucible was wrapped with wire. The wires used in these experiments were high purity Pt, Cu, Ni, Ag (≥99.99%, Alfa Aesar), and 316 stainless steel (99+%). Once the wire was wrapped around the crucible, this was placed inside of a ~30-cm long fused

quartz ampoule (GE214, 19×22 mm) sealed on one end, and a fused quartz endcap was inserted into the tube. The assembly was connected to compression fitting attached to a gate valve and this was transferred out of the glovebox and attached to a high vacuum system for evacuation without the ampoule contents being exposed to atmosphere. The tube was evacuated and purged with ultra-high purity Ar several times followed by a final evacuation step to 10^{-5} Pa where it was sealed with a torch. The ampoule was inserted into a custom-made rocking furnace (Deltech, Denver, CO) and heated at a 30° angle to 1000 °C or 1025 °C at 1 °C min^{-1}. Cooling rates were different for the various experiments and temperatures were monitored by Type-K thermocouples (OMEGA Engineering, Inc., Norwalk, CT) using a data acquisition system (DAQ, HYDRA 2620A, Fluke Corporation, Everett, WA).

2.4 Vertical gradient furnace (VGF) experiments

For the two VGF experiments (Table 2-1), the charge was added to a custom-fabricated 55-mm OD glassy carbon crucible with a 170-mm long tapered wall to a 25-mm deep conical tip from HTW. This was placed into a custom-fabricated 57×61×457 mm fused quartz tube (GE224) with a conical tip to match that on the crucible and a glassy carbon lid was added. Since the tolerance between the inner wall of the ampoule and the outer wall of the crucible was so small, the metal getters were added as cut discs of high purity Cu or Ni (99.999%, Alfa Aesar) on top of the crucible lid. A fused quartz end cap was then inserted and the ampoules were evacuated and sealed as mentioned previously prior to loading into an 18-zone gradient furnace (EDG Sunfire, The Mellen Company, Inc., Concord, NH). Heat treatments were run under a 50 °C gradient and then slow cooled at 1 °C min^{-1}.

2.5 Post heat-treatment sample preparations

Following heat-treatment, the samples were mounted in resin and cut using a CT400 diamond wire saw (Diamond Wire Technology, LLC, Colorado Springs, CO). They were then polished to a < 1-μm finish for microscopy using diamond suspensions and colloidal silica on a vibratory polisher.

2.6 Powder X-ray diffraction

Phase analysis on the material outside of the crucible was conducted with powder X-ray diffraction (P-XRD) using a Bruker® D8 Advance (Bruker AXS Inc., Madison, WI) XRD with Cu K_α emission. The detector used was a LynxEye™ position-sensitive detector with a collection window of 3° 2θ. Scan parameters were 5–70° 2θ with a step of 0.015° 2θ and a 0.3-s dwell at each step. A majority of the material was ground in a Diamonite™ mortar and pestle. Portions of this material were reserved for microscopy.

2.7 Optical microscopy

Optical microscopy was performed on polished cross-sections with a BX51M (Olympus, Center Valley, PA) using cross-polarized light and differential interference contrast filters. Optical micrographs of samples were produced using the Stream image analysis software by stitching higher magnification images into a single higher resolution image. In some cases, this stitching was done in Adobe Photoshop CS6 and Photoshop was used to convert the images into black and white.

2.8 Electron backscatter diffraction

Electron backscatter diffraction (EBSD) was performed on polished cross sections using a JEOL 7600F field emission scanning electron microscope (SEM, JEOL USA, Inc. Peabody, MA) equipped with an Nordlys EBSD camera interfaced with the HKL Channel 5 software package (Oxford Instruments PLC, UK). The EBSD mapping was performed using an accelerating voltage of 20 kV. The CdTe phase was indexed with ICSD#93943 (Rabadanov et al., 2001) (a = 6.486 Å) and CdSe was indexed with ICSD#620423 (Cook, 1968) (a = 4.299 Å, c = 7.010 Å). Post-acquisition data processing was performed by applying minimal data smoothing and removing wild spikes. For some samples, multiple maps were collected to cover the full region of interest and stitched together using the Oxford software.

3.0 Results and Discussion

3.1 CdTe experiments

The original goal of the Pt wire was to hold the lid in place on top of the crucible so that the contents of the crucible would not spill out when the crucible was loaded into the ampoule. However, after the heat-treatment, it was observed that the Pt had reacted with the Te flux to form $PtTe_2$. Pictures of the first experiment are shown in Figure 3-2.

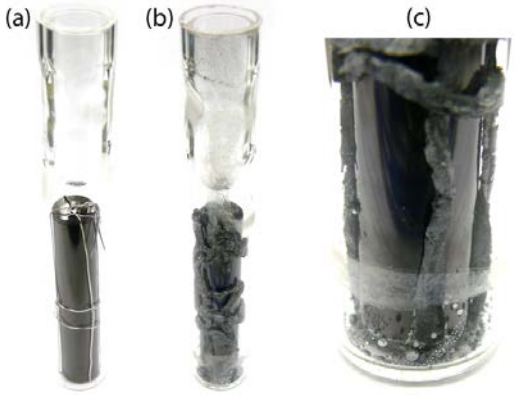

Figure 3-1. Pictures of ITF-1000C-FC-Pt-1 (ITF-1) both (a) before and (b,c) after the heat treatment.

3.1.1 ITF experiments

The thermal profiles for the various cooling rates used for the ITF experiments are shown in Figure 3-3. In addition to these, a 10 °C min^{-1} rate is also shown, which is close to the initial cooling rate of the FC experiments. Optical micrograph collages are shown for a select few of the ITF samples in Figure 3-4.

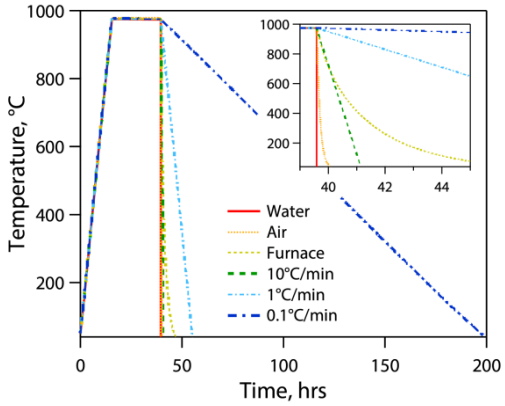

Figure 3-2. Thermal profile for the different cooling rates used during the ITF experiments.

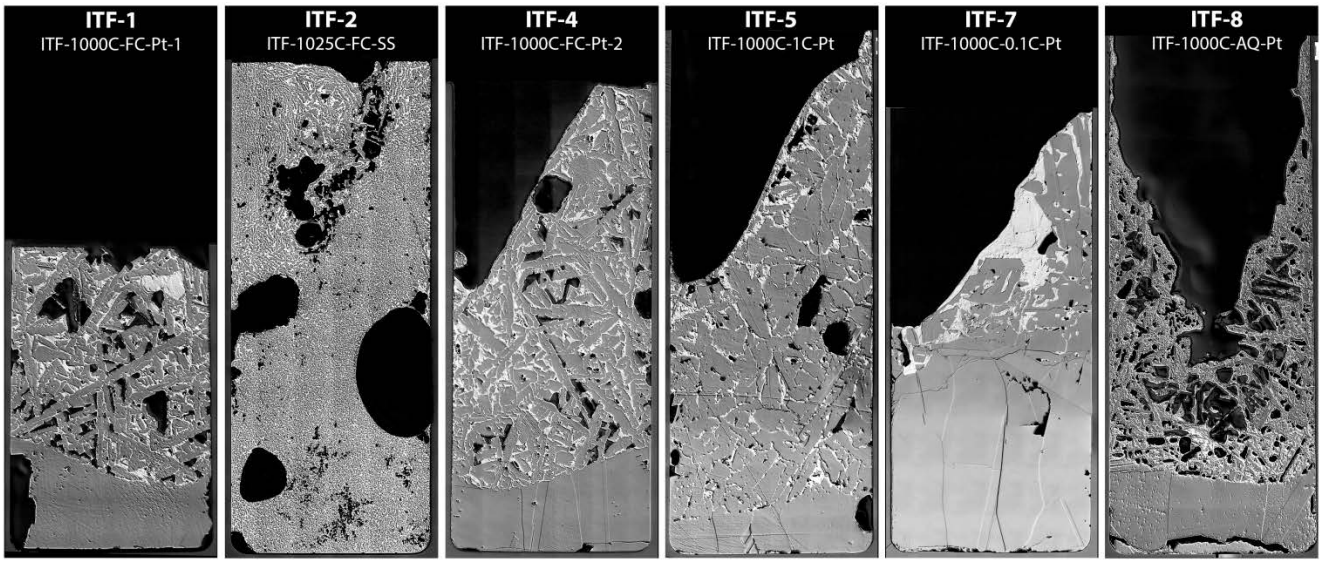

Figure 3-3. Optical collage of select samples. For scale, all samples are shown at ~10-mm diameter.

The P-XRD phase analysis results for the material present in the annulus between the crucible and the ampoule for all ITF experiments are presented in Table 3-2 with corresponding phases detected (Anderko and Schubert, 1954; Bradley, 1924; Davey, 1925; Dobrovol'skii et al., 1972; Forman and Peacock, 1949; Furberg, 1953; Hamasaki et al., 1975; Imanov and Pinsker, 1966; Peacock and Thompson, 1946; Pertlik, 1986; Thomassen, 1929; Woolley and Williams, 1966). In all cases, both CdTe and Te migrated out of the crucible and the Te reacted with the getter while the CdTe remained as CdTe. In all cases, some CdTe was detected as a minor phase except when Ag was used as the getter for ITF-1000C-1C-Ag (69.04 mass% CdTe). In all other cases, the primary phases found were Te-alloys with the original getter material. For the ITF-1025C-FC-SS and ITF-1000C-FC-SS, the primary phase was Te with several secondary Fe-, Cr-, and Mn-alloy phases. The composition of the CdTe layer was evaluated using energy dispersive spectroscopy (EDS) using a JSM-7600 field emission gun scanning electron microscope (see Appendix A), to ensure the produced crystals were free of getter material. EDS results indicated average getter concentrations in the CdTe layer were < 1 mass% and can be found in the supplementary information provided.

Table 3-1. Summary of phases (Anderko and Schubert, 1954; Bradley, 1924; Davey, 1925; Dobrovol'skii et al., 1972; Forman and Peacock, 1949; Furberg, 1953; Hamasaki et al., 1975; Imanov and Pinsker, 1966; Peacock and Thompson, 1946; Pertlik, 1986; Thomassen, 1929; Woolley and Williams, 1966) present in material found outside the crucible in the annulus with P-XRD analysis where "SS" denotes stainless steel. For the VGF entries in the table, the top row designates the material found on top of the crucible lid and the bottom is what was found at the bottom tip of the annulus with masses for each shown in brackets "[ ]" under the 'Other' column.

Sample ID	Alternative ID	Phase (mass%)			Residual sample mass in crucible (g)	Annular material (mass%)
		CdTe	Te	Other		
ITF-1000C-FC-Pt-1	ITF-1	2.95	0.15	96.9 ($PtTe_2$)	9.350	28%
ITF-1025C-FC-SS	ITF-2	18.05	40.99	27.68 ($FeTe_2$), 11.13 (Cr_2Te_3), 0.95 ($MnTe_2$), 1.20 (CrFe)	10.529	19%
ITF-1000C-FC-SS	ITF-3	22.50	39.49	25.35 ($FeTe_2$), 11.52 ($Cr2Te_3$), 0.57 ($MnTe_2$), 0.57 (CrFe)	10.460	19%
ITF-1000C-FC-Pt-2	ITF-4	3.29	1.35	95.36 ($PtTe_2$)	9.372	28%
ITF-1000C-1C-Pt	ITF-5	8.83	6.69	84.48 ($PtTe_2$)	9.369	28%
ITF-1000C-WQ-Pt	ITF-6	11.37	3.95	84.68 ($PtTe_2$)	9.287	28%
ITF-1000C-0.1C-Pt	ITF-7	7.81	16.12	76.07 ($PtTe_2$)	9.255	29%
ITF-1000C-AQ-Pt	ITF-8	25.22	6.81	67.97 ($PtTe_2$)	8.596	34%
ITF-1000C-1C-Cu	ITF-9	23.85	21.63	53.08 (CuTe), 1.44 ($Cu_{2.8}Te_2$)	6.601	49%
ITF-1000C-1C-Ni	ITF-10	14.49	3.12	77.76 ($NiTe_2$), 4.63 (Ni)	7.164	45%
ITF-1000C-1C-Ag	ITF-11	69.04	7.29	23.67 (Ag_7Te_4)	2.089	84%
VGF-8x-1C-Cu	VGF-1	26.77	20.55	52.68 (CuTe) [49.51 g]	110.1	47%
		78.30	10.43	11.27 (CuTe) [77.85 g]		
VGF-8x-1C-Ni	VGF-2	18.87	26.07	55.06 ($NiTe_2$) [42.84 g]	115.3	45%
		27.18	0.11	72.71 ($NiTe_2$) [70.57 g]		

Based on the data shown in Table 3-2 and Figure 3-5, a few trends were observed in the data. For samples cooled at 1 °C min^{-1} using getters of Pt (ITF-1000C-1C-Pt), Ni (ITF-1000C-1C-Ni), Cu (ITF-1000C-1C-Cu), and Ag (ITF-1000C-1C-Ag) shown in Figure 3-5a, the amount of Te in the annulus was highest for Cu (21.63 mass%) and lowest for Ni (3.12 mass%) with Pt (6.69 mass%) and Ag (7.29 mass%) being fairly close to one another. The amount of telluride phases were high for both the Pt and Ni experiments with $PtTe_2$ = 84.48 mass% and $NiTe_2$ = 77.76 mass%, respectively. The amount of CdTe removed from the crucible increased in the order of Pt < Ni < Cu < Ag, with the Ag sample having a drastically higher amount than the other three (Figure 3-5a).

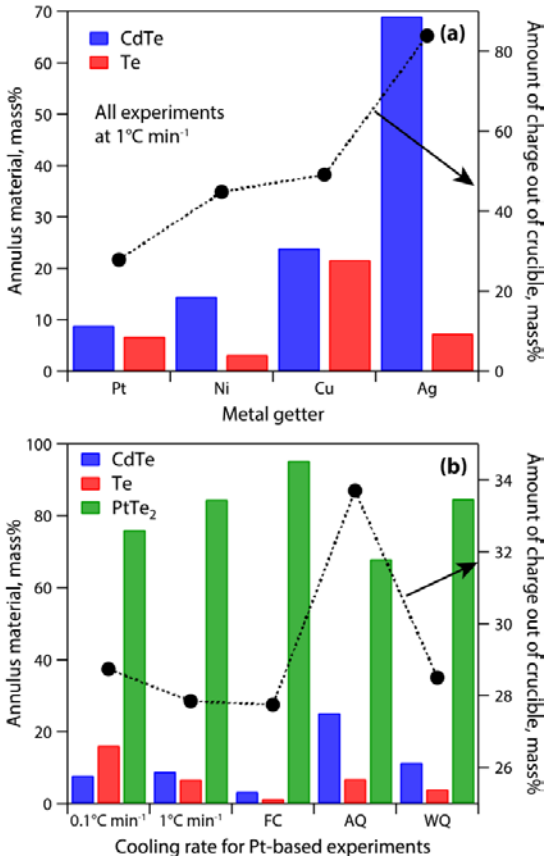

Figure 3-4. Annulus material phase distribution comparisons for (a) all getters run with 1 °C min^{-1} cooling rate and (b) for all Pt samples run at different cooling rates. For both plots, an overlay is provided for the amount of charge that was removed from the crucible into the annulus during the experiment.

When looking at the Pt-based experiments, cooling rates of 0.1 °C min^{-1} (ITF-1000C-0.1C-Pt), 1 °C min^{-1} (ITF-1000C-1C-Pt), furnace cooling (FC; ITF-1000C-FC-Pt-2), air quenching (AQ; ITF-1000C-AQ-Pt), and water quenching (WQ; ITF-1000C-WQ-Pt), the data were similar with some minor differences (Figure 3-5b). In all cases, the only three phases observed were CdTe, Te, and $PtTe_2$ and these amounts varied somewhat for each experiment. The AQ sample seemed like an anomaly when comparing the amount of charge transferred out of the crucible where this data point was noticeably higher (33.7%) than all of the other four experiments (28.2±0.49%). Interestingly, the sample with highest fraction of $PtTe_2$ and lowest of both CdTe and Te was the FC sample, suggesting that this was an optimal cooling temperature for removing the Te flux to the annulus without removing CdTe from the crucible. The EBSD maps for ITF-1000C-0.1C-Pt (RF7) (Figure 3-6) show that the large grains in these samples are of single orientation.

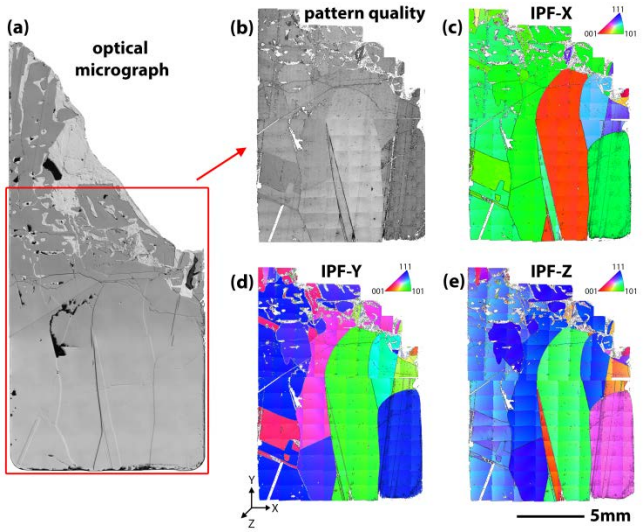

Figure 3-5. (a) Optical micrograph of ITF-1000C-0.1C-Pt (RF-7). (b-e) EBSD collage collected over the region highlighted in (a) including (b) pattern quality map, (c) IPF-X map, (d) IPF-Y map, and (e) IPF-Z map (IPF = inverse pole figure).

3.1.2 VGF experiments

For the VGF experiments, the samples recovered at the base of the crucibles were very large and appeared to be mostly comprised of CdTe with small Te precipitates towards the upper middle of the ingots indicated by brighter spots (Figure 3-7). There were some clear differences in the samples, with the primary one being that no voids were found within the sample run with Cu (VGF-8x-1C-Cu or VGF-1) while the sample run with Ni (VGF-8x-1C-Ni or VGF-2) had numerous regions where voids were observed. The grains found in both samples were larger and are denoted by the differences in surface relief within the grains.

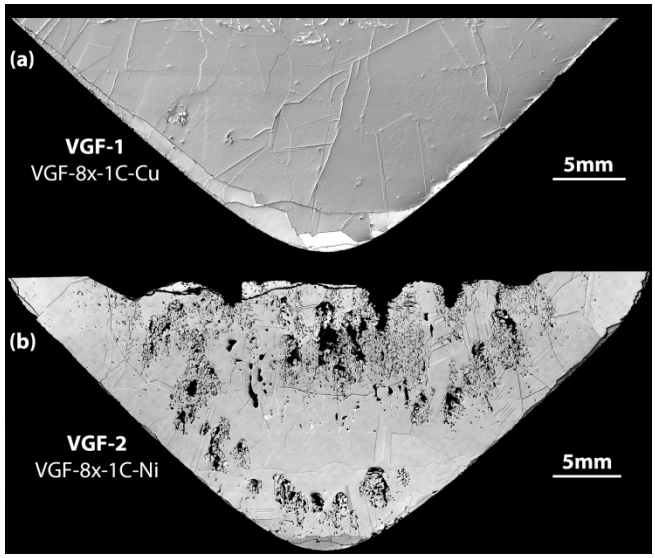

Figure 3-6. Optical micrographs of (a) VGF-8x-1C-Cu (VGF-1) and (b) VGF-8x-1C-Ni (VGF-2).

3.2 CdSe experiments

The results of the CdSe experiments were quite different than those of the CdTe runs. Due to the higher melting temperature of CdSe (1239–1258 °C) (Cook, 1968; Sosovska, 2007) versus 1092 °C for CdTe (Avetissov et al., 2011) the process of producing larger CdSe crystals proved more difficult. The products for CdSe-1 and CdSe-2 made with and without a getter, respectively, yielded pure CdSe according to the P-XRD and EBSD analysis. This is partly due to that fact that, at the 1100 °C processing temperature used for both CdSe experiments, the high volatility of Se resulted in removal of the flux before the charge had fully consolidated into a non-porous product Figure 3-8a. The dynamic flux removal process for CdSe-1 was effective at removing the Se from the crucible by reacting with the Pt to form $PtSe_2$ as determined with P-XRD.

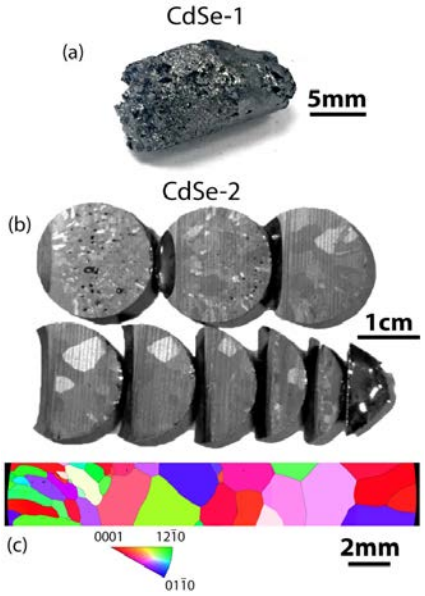

Figure 3-7. Pictures of (a) CdSe-1 and (b) CdSe-2 and (c) an EBSD map (IPF-Z) collage across the CdSe crystal grains of one of the sections cut from CdSe-2.

For experiments CdSe-2, which was run without a crucible, the Se vapor was always in contact with the CdSe melt during the course of the experiment and the sample had a thin layer of Se on the top surface upon cooling. This presence of the Se layer was due to a combination of the CdSe freezing before the Se during cooling and because the density of CdSe (5.67 g/cm^3) is higher than that of Se (4.79 g/cm^3) (Campbell and Epstein, 1942; Cook, 1968). The resulting product was fully consolidated with low porosity and many visible grains (Figure 3-8b). The EBSD map shown in Figure 3-8c revealed that the grains were all CdSe without Se in the grain boundaries.

While the CdSe can be grown well below the melting temperature (1239–1258 °C) (Cook, 1968; Sosovska, 2007) using a Se flux with and without a getter material, the use of the getter was not as effective as it was with the CdTe. This was partly due to the higher volatility of Se versus that of Te, resulting in less residence time within the crucible. Thus, the experiment performed without the getter was more successful.

4.0 Conclusions

The results from these studies show that the flux-assisted in situ dynamic flux removal process for growing CdTe was very effective at yielding large crystal grains, although not as effective for the CdSe system. The process worked well for experimental setups at small scales (ITF) and at much larger scales (VGF). With the various getters that were evaluated for the CdTe ITF experiments, the most effective at removing the excess Te flux was the Pt getter. For the Pt, Ni, Cu, and Ag experiments, $PtTe_2$, $NiTe_2$, CuTe, and Ag_7Te_4 were formed, respectively. For the experiment with the SS getter, a variety of phases were observed including $FeTe_2$, Cr_2Te_3, $MnTe_2$, and CrFe. When the VGF experiments were conducted on an 8× scale from the ITF experiments, the Cu getter proved more successful than the Ni getter at producing a consolidated product with few voids and nicely sized grains, demonstrating the scalability of this process.

This approach of using flux-assisted growth provides an opportunity to process melts at much lower temperatures than those run at stoichiometric (i.e., CdTe, CdSe) compositions and this provides some safety margins not otherwise available. The lower processing temperatures also reduce the volatility and selective decomposition of the more volatile constituents in each system during the melting process. The concept of using a getter to remove the flux preferentially in situ advances the process by helping prevent build-up of the flux material within the grain boundaries of the CdTe or CdSe crystal grains. This approach could likely be extrapolated to other systems in the future.

5.0 References

Anderko, K. and K. Schubert. 1954. "The system copper-tellurium." *Zeitschrift fuer Metallkunde* **45**:371-78.

Avetissov, I. C., E. A. Sukhanova, A. V. Khomyakov, A. Y. Zinovjev, V. A. Kostikov, and E. V. Zharikov. 2011. "Simulation and crystal growth of CdTe by axial vibration control technique in Bridgman configuration." *Journal of Crystal Growth* **318**(1):528-32.

Becker, E. M., C. E. Seifert, M. J. Myjak, L. E. Erikson, S. J. Morris, D. T. Balvage, and R. P. Lundy. 2011. Performance characteristics of pixelated CZT crystals used on the GammaTracker project. In *Proceedings of Proc. SPIE*. eds. LA Franks, RB James and A Burger, vol. 8142, pp. 81420F-1-17.

Berlincourt, D., H. Jaffe, and L. R. Shiozawa. 1963. "Electroelastic properties of the sulfides, selenides, and tellurides of zinc and cadmium." *Physical Review* **129**(3):1009-17.

Bradley, A. J. 1924. "The crystal structures of the rhombohedral forms of selenium and tellurium." *Philosophical Magazine* **48**:477-96.

Burger, A., M. Groza, Y. Cui, D. Hillman, E. Brewer, A. Bilikiss, G. W. Wright, L. Li, F. Lu, and R. B. James. 2003. "Characterization of large single-crystal gamma-ray detectors of cadmium zinc telluride." *Journal of Electronic Materials* **32**(7):756-60.

Burger, A., I. Shilo, and M. Schieber. 1983. "Cadmium selenide: A promising novel room temperature radiation detector." *IEEE Transactions on Nuclear Science* **30**(1):368-70.

Campbell, A. N. and S. Epstein. 1942. "The Density of Selenium." *Journal of the American Chemical Society* **64**(11):2679-80.

Carmody, M. and A. Gilmore. 2011. *High Efficiency Single Crystal CdTe Solar Cells*. NREL/SR-5200-51380, EPIR Technologies Bolingbrook, IL.

Chu, T. L. and S. S. Chu. 1993. "Recent progress in thin-film cadmium telluride solar cells." *Progress in Photovoltaics* **1**(1):31-42.

Cook, W. R. J. 1968. "The CdS-MnS and CdSe-MnSe phase diagrams." *Journal of the American Ceramic Society* **51**(9):518-20.

Dabbousi, B. O., J. Rodriguez-Viejo, F. V. Mikulec, J. R. Heine, H. Mattoussi, R. Ober, K. F. Jensen, and M. G. Bawendi. 1997. "(CdSe)ZnS core−shell quantum dots: synthesis and characterization of a size series of highly luminescent nanocrystallites." *The Journal of Physical Chemistry B* **101**(46):9463-75.

Davey, W. P. 1925. "Precision Measurements of the Lattice Constants of Twelve Common Metals." *Physical Review* **25**(6):753-61.

Dobrovol'skii, V. D., S. M. Karal'nik, and A. V. Koval. 1972. "X-ray spectral study of some alloys in relation to deviations form the additivity rule." *Metallofizika (Akademiya Nauk Ukrainskoi SSR, Institut Metallofiziki)* **41**:73-77.

Forman, S. A. and M. A. Peacock. 1949. "Crystal structure of rickardite, $Cu_{4-x}Te_2$." *American Mineralogist* **34**:441-51.

Furberg, S. 1953. "The system manganese-tellurium." *Acta Chemica Scandinavica* **7**:693-94.

Gessert, T. A. and D. Bonnet. 2015. "Polycrystalline Cadmium Telluride Photovoltaic Devices." In *Clean Electricity from Photovoltaics, 2nd ed.*, eds. MD Archer and MA Green, pp. 209-44. Imperial College Press, London.

Greenberg, J. H. 2003. "P–T–X phase equilibrium and vapor pressure scanning of non-stoichiometry in the Cd-Zn-Te system." *Progress in Crystal Growth and Characterization of Materials* **47**(2-3):196-238.

Hamasaki, T., T. Hashimoto, Y. Yamaguchi, and H. Watanabe. 1975. "Neutron diffraction study of Cr_2Te_3 single crystal." *Solid State Communications* **16**(7):895-97.

Henager, C. H., K. J. Alvine, M. Bliss, B. J. Riley, and J. A. Stave. 2015. "The influence of constitutional supercooling on the distribution of Te-particles in melt-grown CZT." *Journal of Electronic Materials* **44**(11):4604-21.

Imanov, R. M. and Z. G. Pinsker. 1966. "Determination of the crystal structure of the hexagonal phase in the Ag-Te system." *Kristallografiya* **11**(2):182-90.

Johnson, C. 1968. Electrooptic effect in CdTe at 23.35 and 27.95 microns. In *Proceedings of Proc. IEEE*. eds. ME Van Valkenburg, vol. 56, pp. 1719-20, IEEE.

Johnson, C. J., G. H. Sherman, and R. Weil. 1969. "Far infrared measurement of the dielectric properties of GaAs and CdTe at 300 K and 8 K." *Appl. Opt.* **8**(8):1667-72.

Karakaya, I. and W. T. Thompson. 1991. "The Ag–Te (silver–tellurium) system." *Journal of Phase Equilibria* **12**(1):57-63.

Knoll, G. F. 2000. *Radiation Detection and Measurement, 3rd ed.*, John Wiley & Sons, Inc.

Koohpayeh, S. M. 2016. "Single crystal growth by the traveling solvent technique: A review." *Progress in Crystal Growth and Characterization of Materials*.

Lee, S. Y. and P. Nash. 1991. "Ni-Te (nickel-tellurium)." In *Phase diagrams of binary nickel alloys*, ed. P Nash, pp. 330-38. Materials Park, Ohio.

Mandel, G. and F. F. Morehead. 1964. "Efficient electroluminescence from *p-n* junctions in CdTe at 77 K." *Applied Physics Letters* **4**:143-45.

Mangin, J. and P. Veber. 2008. "$PtTe_2$: Potential new material for the growth of defect-free TeO_2 single crystals." *Journal of Crystal Growth* **310**(12):3077-83.

Manna, L., E. C. Scher, and A. P. Alivisatos. 2000. "Synthesis of soluble and processable rod-, arrow-, teardrop-, and tetrapod-shaped CdSe nanocrystals." *Journal of the American Chemical Society* **122**(51):12700-06.

McArthur, D. A. and R. A. McFarlane. 1970. "Optical mixing in cadmium telluride using the pulsed water vapor laser." *Appl. Phys. Lett.* **16**:452-54.

Mongy, A. A.-E. 2004. "Preparation and characterization of CdSe single crystal." *Egyptian Journal of Solids* **27**(1):111-19.

Okamoto, H. and T. B. Massalski. 1994. "Binary alloy phase diagrams requiring further studies." *Journal of Phase Equilibria* **15**(5):500-21.

Park, S. H., M. P. Casey, and J. Falk. 1993. "Nonlinear optical properties of CdSe quantum dots." *Journal of Applied Physics* **73**(12):8041-45.

Peacock, M. A. and R. M. Thompson. 1946. "Melonite from Quebec and the crystal structure of $NiTe_2$." *University of Toronto Studies, Geological Series* **50**:63-73.

Pertlik, F. 1986. "Strukturvergeinerung der synthetischen Verbindung $FeTe_2$ (Frohbergit)." *Anzeigerder Osterreichischen Akademie der Wissenschaften, math.-naturwiss. Klasse* **123**:123-25.

Qu, L. and X. Peng. 2002. "Control of photoluminescence properties of CdSe nanocrystals in growth." *Journal of the American Chemical Society* **124**(9):2049-55.

Rabadanov, M. K., I. A. Verin, Y. M. Ivanov, and V. I. Simonov. 2001. "Refinement of the atomic structure of CdTe single crystals." *Crystallography Reports* **46**(4):636-41.

Rubenstein, M. 1966. "Solubilities of some II-VI compounds in bismuth." *J. Electrochem. Soc.* **113**(6):623-24.

Rubenstein, M. 1968. "Solution growth of some II-VI compounds using tin as a solvent." *Journal of Crystal Growth* **3**(4):309-12.

Schaake, H. F., J. H. Tregilgas, J. D. Beck, M. A. Kinch, and B. E. Gnade. 1985. "The effect of low temperature annealing on defects, impurities, and electrical properties of (Hg,Cd)Te." *Journal of Vacuum Science and Technology A* **3**(1):143-49.

Shiraki, H., M. Funaki, Y. Ando, S. Kominami, K. Amemiya, and R. Ohno. 2007. "Improvement of the productivity in the growth of CdTe single crystal by THM for the new PET system." *IEEE Nucl. Sci. Symp.* **3**:1783-87.

Sosovska, S. M. 2007. "The quasi-ternary CdSe-Ga_2Se_3-Sb_2Se_3 system." *Polish Journal of Chemistry* **81**(4):505-13.

Stafsudd, O. M. and D. H. Alexander. 1971. "Continuous second harmonic generation in single-crystal cadmium telluride." *Applied Optics* **10**(11):2566-67.

Thomassen, L. 1929. "The crystal structure of some binary compounds of the platinum metals." *Zeitschrift fur Physikalische Chemie* **2**(B):349-79.

Triboulet, R. and P. Siffert, eds. 2010. *CdTe and Related Compounds; Physics, Defects, Hetero- and Nano-structures, Crystal Growth, Surfaces and Applications*. Elsevier, UK.

Wald, F. V. 1977. "Applications of CdTe. A review." *Revue de Physique Appliquee* **12**(2):277-90.

Woodbury, H. H. and R. S. Lewandowski. 1971. "Improved sealed-ingot zone refining technique for growth of CdTe crystals." *Journal of Crystal Growth* **10**(1):6-12.

Woolley, J. C. and E. W. Williams. 1966. "Some cross-substitutional alloys of CdTe." *Journal of the Electrochemical Society* **113**(9):889-901.

Wuister, S. F., I. Swart, F. van Driel, S. G. Hicky, and C. de Mello Donega. 2003. "Highly luminescent water-soluble CdTe quantum dots." *Nano Letters* **3**(4):503-07.

Appendix A

EDS Analysis of Getter Concentrations in CdTe Crystals

A.1 ITF-1000C-1C-Pt ($Cd_{70}Te_{30}$, ITF-5 with Pt-wire)

Table A-1. EDS Results for ITF-1000C-1C-Pt ($Cd_{70}Te_{30}$, ITF-5 with Pt-wire).

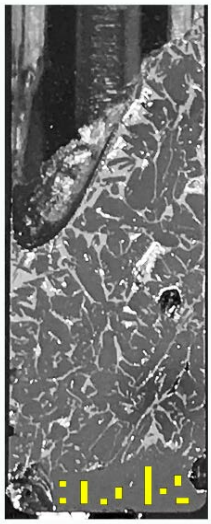

Location	Composition in mass%					
	Cd	Te	Pt	Al	Si	Total
1	47.43	52.34	**0.00**	0.13	0.10	100.0
2	47.42	52.37	**0.00**	0.11	0.10	100.0
3	47.41	52.41	**0.04**	0.05	0.09	100.0
4	47.50	52.27	**0.01**	0.09	0.12	100.0
5	47.43	52.34	**0.04**	0.08	0.11	100.0
6	47.37	52.36	**0.03**	0.13	0.11	100.0
7	47.37	52.44	**0.01**	0.07	0.10	100.0
8	47.50	52.23	**0.06**	0.11	0.09	100.0
9	47.38	52.37	**0.04**	0.08	0.13	100.0
Max	*47.50*	*52.44*	***0.06***	*0.13*	*0.13*	-
Min	*47.37*	*52.23*	***0.00***	*0.05*	*0.09*	-
Average	*47.42*	*52.35*	***0.03***	*0.10*	*0.11*	-
Std. Dev.	*0.05*	*0.06*	***0.02***	*0.03*	*0.01*	-

NOTE: Minimum Detectable Limit (MDL) for EDS is typically ~0.1 mass%, the reported values indicate Pt is < MDL.

**Yellow marks are approximate and indicate the center of the spectrum area.*

A.2 ITF-1000C-1C-Cu ($Cd_{70}Te_{30}$, ITF-9 with Cu-wire)

Table A-2. EDS Results for ITF-1000C-1C-Cu ($Cd_{70}Te_{30}$, ITF-9 with Cu-wire).

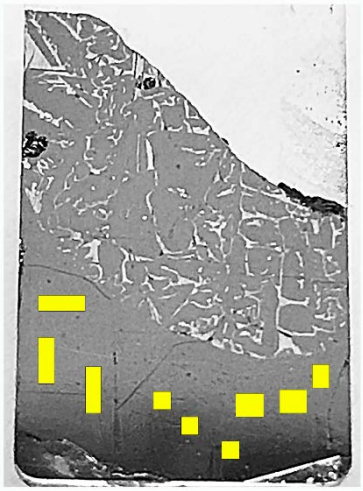

Location	Composition in mass%					
	Cd	Te	Cu	Al	Si	Total
1	47.26	52.35	**0.18**	0.05	0.16	100.0
2	47.27	52.25	**0.21**	0.09	0.18	100.0
3	47.37	52.24	**0.17**	0.08	0.13	100.0
4	47.18	52.37	**0.14**	0.17	0.13	100.0
5	47.20	52.23	**0.34**	0.05	0.18	100.0
6	47.38	52.23	**0.20**	0.04	0.15	100.0
7	47.30	52.38	**0.16**	0.03	0.12	100.0
8	47.28	52.34	**0.17**	0.07	0.13	100.0
9	47.32	52.26	**0.19**	0.10	0.12	100.0
Max	47.38	52.38	**0.34**	0.17	0.18	-
Min	47.18	52.23	**0.14**	0.03	0.12	-
Average	47.29	52.29	**0.20**	0.08	0.15	-
Std. Dev.	0.07	0.06	**0.06**	0.04	0.02	-

**Yellow marks are approximate and indicate the center of the spectrum area.*

A.3 ITF-1000C-1C-Ni ($Cd_{70}Te_{30}$, ITF-10 with Ni-Wire)

Table A-3. EDS Results for ITF-1000C-1C-Ni ($Cd_{70}Te_{30}$, ITF-10 with Ni-Wire).**

Location	Composition in mass%					
	Cd	Te	Ni	Al	Si	Total
1	47.34	51.91	**0.53**	0.05	0.16	100.0
2	47.05	51.49	**1.23**	0.05	0.17	100.0
3	47.09	51.8	**0.88**	0.10	0.13	100.0
4	47.22	52.13	**0.45**	0.10	0.11	100.0
5	47.18	52.07	**0.56**	0.06	0.13	100.0
6	46.85	51.71	**1.21**	0.07	0.17	100.0
7	46.97	51.64	**1.16**	0.10	0.13	100.0
8	47.05	52.03	**0.73**	0.08	0.11	100.0
9	46.73	51.27	**1.78**	0.10	0.12	100.0
Max	47.34	52.13	**1.78**	0.10	0.17	-
Min	46.73	51.27	**0.45**	0.05	0.11	-
Average	47.05	51.78	**0.95**	0.08	0.14	-
Std. Dev.	0.19	0.29	**0.44**	0.02	0.02	-

**Yellow marks are approximate and indicate the center of the spectrum area.*

**See below for information on sample backgrounds

A.4 ITF-1000C-1C-Ag ($Cd_{70}Te_{30}$, ITF-11 with Ag-Wire)

Table A-4. EDS Results for ITF-1000C-1C-Ag ($Cd_{70}Te_{30}$, ITF-11 with Ag-Wire).

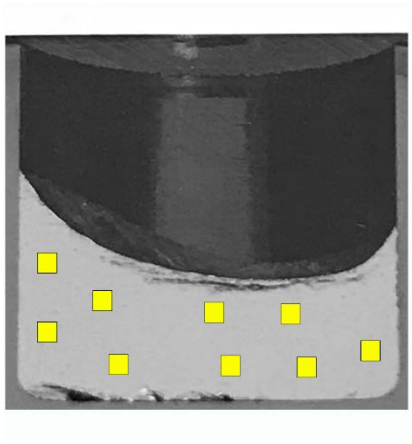

Location	Composition in mass%					
	Cd	Te	Ag	Al	Si	Total
1	46.79	52.32	**0.64**	0.05	0.19	100.0
2	46.99	52.27	**0.57**	0.04	0.13	100.0
3	47.11	52.31	**0.42**	0.07	0.09	100.0
4	47.12	52.21	**0.45**	0.11	0.11	100.0
5	46.74	52.52	**0.54**	0.01	0.19	100.0
6	47.18	52.33	**0.31**	0.05	0.13	100.0
7	47.09	52.25	**0.49**	0.04	0.13	100.0
8	46.95	52.39	**0.47**	0.08	0.11	100.0
9	47.14	52.31	**0.36**	0.09	0.10	100.0
Max	47.18	52.52	**0.64**	0.11	0.19	-
Min	46.74	52.21	**0.31**	0.01	0.09	-
Average	47.01	52.32	**0.48**	0.06	0.13	-
Std. Dev.	0.16	0.09	**0.10**	0.03	0.04	-

**Yellow marks are approximate and indicate the center of the spectrum area.*

A.5 Discussion of backgrounds and peak interferences

ITF-5, ITF-9, and ITF-11 (i.e., Pt, Cu and Ag getters, respectively) were free of significant peak overlap when EDS spectral overlays were examined. ITF-10 (Ni getter), however, did exhibit the potential for peak overlap to be falsely skewing the Ni quantification as shown below in Figure A-1.

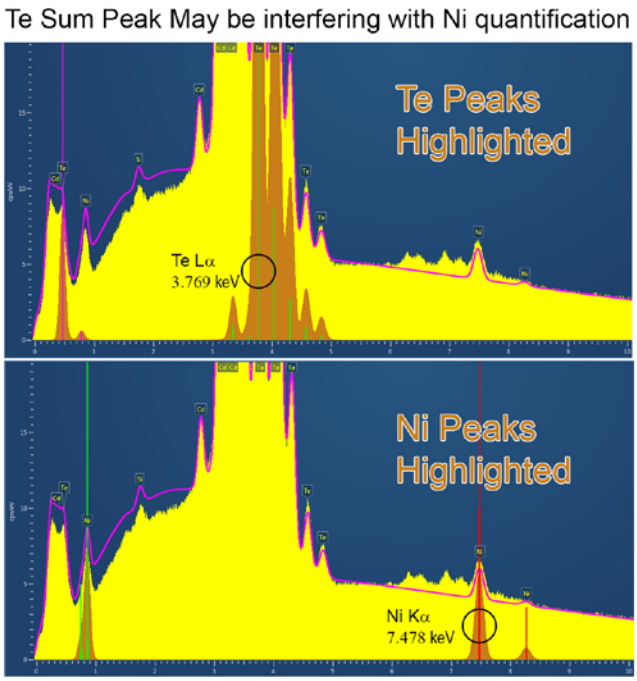

Figure A-1. EDS spectra from ITF-10 (Ni getter; EDS region 2). Locations of the primary Te and Ni peaks illustrate that summation of 2× the energy from a Te Lα peak very nearly overlaps the Ni Kα peak.

Because some fraction of the Ni signal observed in the spectra obtained from ITF-10 may be resulting from a Te sum peak, the Ni concentration was quantified in samples ITF-5, ITF-9, and ITF-11 (free of Ni) to see if an increased Ni signal was visible. Table A-5 shows the average Ni content measured in these samples was 0.23 ± 0.09 mass%, which is believed to be an artificial background concentration. The average Ni concentration as measured from these samples was background subtracted from the results initially presented in Section A.3 and is shown in Table A-6.

Table A-5. Forced Ni background measured from ITF-5, ITF-9, and ITF-11.

ID	#	Composition in mass%								
		Cd	Te	Ni	Cu	Ag	Al	Si	Pt	Total
ITF-5 (Pt)	1	47.35	52.23	0.18	-	-	0.13	0.10	0.00	100
	2	47.35	52.27	0.16	-	-	0.11	0.10	0.00	100
	3	47.36	52.32	0.14	-	-	0.05	0.09	0.04	100
	4	47.42	52.16	0.20	-	-	0.09	0.12	0.01	100
	5	47.34	52.22	0.21	-	-	0.08	0.11	0.04	100
	6	47.31	52.27	0.16	-	-	0.13	0.11	0.03	100
	7	47.29	52.33	0.19	-	-	0.07	0.10	0.01	100
	8	47.42	52.12	0.19	-	-	0.11	0.09	0.06	100
	9	47.31	52.26	0.17	-	-	0.08	0.13	0.04	100
ITF-9 (Cu)	1	47.17	52.21	0.21	0.20	-	0.05	0.16	-	100
	2	47.19	52.12	0.20	0.22	-	0.09	0.18	-	100
	3	47.26	52.08	0.25	0.19	-	0.08	0.13	-	100
	4	47.08	52.23	0.23	0.16	-	0.17	0.13	-	100
	5	47.03	52.00	0.37	0.38	-	0.05	0.18	-	100
	6	47.16	51.9	0.51	0.25	-	0.04	0.15	-	100
	7	47.14	52.15	0.36	0.19	-	0.03	0.12	-	100
	8	47.12	52.13	0.34	0.20	-	0.07	0.13	-	100
	9	47.14	52.01	0.40	0.22	-	0.10	0.12	-	100
ITF-11 (Ag)	1	46.75	52.25	0.12	-	0.64	0.05	0.19	-	100
	2	46.91	52.16	0.19	-	0.57	0.04	0.13	-	100
	3	47.02	52.17	0.23	-	0.42	0.07	0.09	-	100
	4	47.04	52.09	0.19	-	0.45	0.11	0.11	-	100
	5	46.68	52.43	0.14	-	0.54	0.01	0.19	-	100
	6	47.07	52.18	0.26	-	0.31	0.05	0.13	-	100
	7	47.02	52.16	0.16	-	0.49	0.04	0.13	-	100
	8	46.86	52.26	0.22	-	0.47	0.08	0.11	-	100
	9	47.09	52.24	0.13	-	0.36	0.09	0.10	-	100
				Max	0.51					
				Min	0.12					
				Average	**0.23**					
				Std. Dev.	**0.09**					

Table A-6. ITF-10 (Ni getter) background subtraction (Ni correction).

Location	Composition in mass%
	Ni–Background Corrected
1	0.30
2	1.00
3	0.65
4	0.22
5	0.33
6	0.98
7	0.93
8	0.50
9	1.55
Max	**1.55**
Min	**0.22**
Average	**0.72**
Std. Dev.	**0.43**

**Yellow marks are approximate and indicate the center of the spectrum area.*

A.6 Summary of Getter Concentrations for ITF-5, ITF-9, ITF-10, and ITF-11

Table A-7. Summary of getter concentrations measured by EDS.

	Pt Getter	Cu Getter	Ni Getter	Ag Getter
Specimen Image	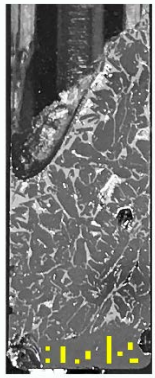	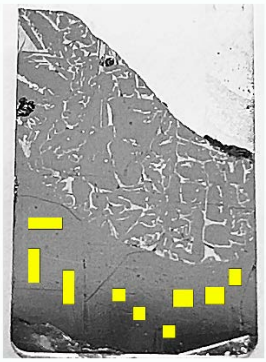		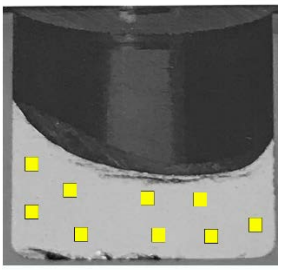
	Concentration in Mass%			
Average ± Std. Dev.	**<MDL*** 0.03 ± 0.02	0.2 ± 0.06	Bkg. Corrected 0.72 ± 0.43	0.48 ± 0.1
Max	0.06	0.34	1.55	0.64
Min	0.00	0.14	0.22	0.31

**MDL = Minimum Detectable Limit*

Pacific Northwest
NATIONAL LABORATORY

www.pnnl.gov

902 Battelle Boulevard
P.O. Box 999
Richland, WA 99352
1-888-375-PNNL (7665)

U.S. DEPARTMENT OF
ENERGY